ECS | The Electrochemical Society
Advancing solid state & electrochemical science & technology

Hydrogen Crossover in PEM Water Electrolysis at Current Densities up to 10 A cm^{-2}

View the article online for updates and enhancements.

Hydrogen Crossover in PEM Water Electrolysis at Current Densities up to 10 A cm⁻²

Agate Martin, Patrick Trinke, Boris Bensmann,[z] and Richard Hanke-Rauschenbach

Leibniz University Hannover, Institute of Electric Power Systems, 30167 Hannover, Germany

Hydrogen crossover poses a critical issue in terms of the safe and efficient operation in polymer electrolyte membrane water electrolysis (PEMWE). The impact of key operating parameters such as temperature and pressure on crossover was investigated in the past. However, many recent studies suggest that the relation between the hydrogen crossover flux and the current density is not fully resolved. This study investigates the hydrogen crossover of PEMWE cells using a thin Nafion 212 membrane at current densities up to 10 A cm⁻² and cathode pressures up to 10 bar, by analysing the anode product gas with gas chromatography. The results show that the hydrogen crossover flux generally increases over the entire current density range. However, the fluxes pass through regions with varying slopes and flatten in the high current regime. Only considering hydrogen diffusion as the single transport mechanism is insufficient to explain these data. Under the prevailing conditions, it is concluded that the electro-osmotic drag of water containing dissolved hydrogen should be considered additionally as a hydrogen transport mechanism. The drag of water acts opposite to hydrogen diffusion and has an attenuating effect on the hydrogen crossover in PEMWE cells with increasing current densities.

This study covers the hydrogen crossover characteristics in polymer electrolyte membrane water electrolysis (PEMWE) at high current densities up 10 A cm⁻².

The assessment of hydrogen loss mechanisms is important for establishing PEM water electrolyzers as an efficient tool for the production of green hydrogen.[1,2] Due to various loss mechanisms, such as leakages and the recombination of hydrogen and oxygen at the cathode, the faradaic efficiency in PEMWE is less than unity.[3–5] The probably most important loss of hydrogen is caused by the diffusion of the evolved hydrogen dissolved in water through the membrane into the anode compartment.[6–9] This effect is known as hydrogen crossover. Especially at part load, the so-formed hydrogen in oxygen mixtures can reach hydrogen contents above 4 vol%, which pose a critical safety issue due to the risk of explosion.[6,8,10,11]

For the investigation of fundamental pressure and temperature relations, hydrogen crossover was first evaluated by permeation experiments at zero current.[7,12,13] In the recent years, hydrogen crossover was investigated at electrolysis conditions by analyzing the hydrogen content in the anode product gas, whereby an increase in hydrogen crossover with increasing current densities was observed. Trinke *et al.*[7,14–16] explain this effect with an increase in the dissolved hydrogen concentration, which results from mass transport limitations within the cathode catalyst layer. This theory was supported by varying the ionomer content in the cathode catalyst layer.[14] It was shown that higher ionomer contents lead to increased mass transport resistances, which in turn result in an increasing supersaturation of water with hydrogen and thus, in higher crossover fluxes.[14] Moreover, Martin *et al.*[17] showed that an increased compression of the cathode leads to similar observable effects.

Generally, hydrogen crossover studies at electrolysis conditions with moderate current densities up to 2 A cm⁻² and thick perfluorosulfonic acid membranes (fumea EF-40 ∼ 240 μm, Nafion 117 ∼ 178 μm, Nafion 115 ∼ 127 μm) revealed a linear relation between the hydrogen crossover flux and current density.[3,4,6,11,14–16]

More recent studies have used thinner Nafion 212 membranes (51 μm) at higher current densities up to 5 A cm⁻².[13,17–19] Compared to the earlier mentioned studies, the usage of thinner membranes generally results in higher anodic hydrogen contents. Further, the relation between the crossover flux and the current density follows a stronger than linear growing function. This functional relation can only partially be explained by known, theoretical approaches, such

as the growing supersaturation with hydrogen at increasing current densities, and the resulting increased driving force for diffusion. However, the former approaches fail to explain other parts of the data, such as the flattening of the hydrogen crossover flux with the further increase of current density or at enhanced cathode pressures.[13,17,20] Thus, it has to be assumed that under these conditions, yet unknown effects happen. This will be considered in more detail within this contribution.

For this purpose, the hydrogen crossover characteristics of a catalyst coated membrane (CCM) based on Nafion 212 is investigated at current densities up to 10 A cm⁻² and at cathode pressures up to 10 bar. The investigation at these pressure levels is particularly interesting in an industrial context, whereas the high current densities are less important in this context and primarily serve to explore the effects on hydrogen crossover.

After presenting the experimental details for this study, an insight into the polarisation behaviour of the examined PEMWE cell is given. Then, a detailed analysis of the impact of the high applied current densities on hydrogen crossover at ambient and at elevated cathode pressures is performed.

Experimental

Material and cell setup.—A 4 cm² cell by Fraunhofer ISE[21] was equipped with a 5.95 mm insulation frame for the anode and a 5.14 mm frame for the cathode. A commercially available CCM based on Nafion 212 (1 mg cm⁻² Pt/C, 2 mg cm⁻² Ir black, Hiat gGmbh) was assembled in the cell. For the anode side, a porous transport layer (PTL) made of sintered titanium fibers (1 mm, 2GDL40–1.00, Bekaert) was ultra-sonicated for 10 min in de-ionised water before usage. A carbon paper with hydrophobic treatment (H23I2, now available as E20H, Freudenberg SE) was used as the cathode PTL.

The cell was assembled in dry state. The cell was thermally conditioned by recirculating water through the anode at 80 °C. Then, the compression force of 3 kN was applied. A minimum contact pressure on the active area of 3.3 MPa is estimated, when a homogeneous distribution of the force on the active cell area and the surrounding gaskets is assumed. Please refer to Ref. 17 for more details on the cell setup and the distribution of contact pressure.

Testing periphery.—After cell assembly, the cell was mounted into an electrolysis test station (E100, Greenlight Innovation). Thermal sensors were placed at the electrode endplates. Only the anode side of the cell was supplied with de-ionised water

[z]E-mail: boris.bensmann@ifes.uni-hannover.de

(80 ml min^{-1} at 80 °C). The resistivity of the water in the test station was $\geqslant 2$ MΩ cm. Here, we would like to highlight the importance of naming the resistivity or conductivity of the de-ionised water used for PEMWE measurements for future works, since it has a significant impact on the cell's performance.[22–24] Manufacturer of electrolyzer systems (e.g. ProtonOnSite,[25,26] Proton Energy Systems[27]) demand a minimum water resistivity of 1 MΩ cm, but recommend a resistivity of greater than 10 MΩ cm. Our own experience shows that PEMWE cells degrade noticeably below the 1 MΩ cm limit. Therefore, we encourage our readers to monitor the minimum resistance continuously.

A SP150 potentiostat equipped with a 100 A booster (current accuracy: 0.5% full scale range, BioLogic) was used as the current source. For the investigation of the hydrogen crossover during electrolysis, the dried product gas was supplied to a gas chromatograph (GC, 490 µGC, Agilent). Helium was used as a carrier gas. In order to ensure safe gas mixtures at low current densities and high cathode pressures, an additional constant oxygen mass flow of 0.06 g min^{-1} ($N_{O_2}^{dil} = 3.125 \cdot 10^{-5}$ mol s^{-1}) was added with a mass flow controller (EL-Flow Prestige, Bronkhorst) to dilute the anode product stream directly behind the cell outlet.

From the diluted, then measured hydrogen content at the GC $\phi_{H_2}^{GC}$, the hydrogen crossover flux $N_{H_2}^{cross}$ is obtained with Eq. 1. Then, Eq. 2 is used to calculate the actual hydrogen content ϕ_{H_2} (see Ref. 17 for details), where $N_{O_2}^{evo} = \frac{i}{4 \cdot F}$ refers to the evolved amount of oxygen by the anodic half-cell reaction.

$$N_{H_2}^{cross} = \frac{\phi_{H_2}^{GC}(N_{O_2}^{evo} + N_{O_2}^{dil})}{1 - \phi_{H_2}^{GC}} \quad [1]$$

$$\phi_{H_2} = \frac{N_{H_2}^{cross}}{N_{H_2}^{cross} + N_{O_2}^{evo}} = \frac{\phi_{H_2}^{GC}(N_{O_2}^{evo} + N_{O_2}^{dil})}{N_{O_2}^{evo} + \phi_{H_2}^{GC} \cdot N_{O_2}^{dil}} \quad [2]$$

Measurement protocol.—Before beginning the actual measurements, the cell was thermally conditioned by recirculating the anode feed water at the operating temperature (80 °C), followed by a polarized conditioning phase at 3 A cm^{-2} for six hours. The conditioning was followed by one measurement block for characterizing the hydrogen crossover and one measurement block for measuring the polarisation behaviour. These two blocks were repeated at each investigated cathode pressure level (1 bar, 4 bar, 7 bar, 10 bar). The anode pressure remained at 1 bar for the entire investigation. The used measurement protocol was based on Ref. 17.

The hydrogen crossover was determined during electrolysis operation by analysing the dried anode product gas via GC. A galvanostatic profile with steps between 0.25 … 10 A cm^{-2} was applied. This cycle was repeated twice. The time intervals for each step were based on previous studies,[14,15,17,28] until a constant hydrogen in oxygen value was reached (3 h for the lowest current density of 0.25 A cm^{-2} down to 1 h starting at a current density of 2 A cm^{-2}).

The polarization behaviour of the cell was measured three times with a galvanostatic step profile with current steps between 0.01 … 10 A cm^{-2} and a holding time of 10 s per step. Each current step was followed by an electrochemical impedance measurement for determining the high frequency resistance R_{HF}. Here, the frequency range was set from 100 kHz to 100 Hz and the amplitude was set to 10% of the DC current. R_{HF} was then identified by the interpolation of the Nyquist plots with the intercept of the real axis.

Results and Discussion

For the sake of completeness, a brief insight into the polarisation behaviour of the investigated PEMWE cell is given before analyzing
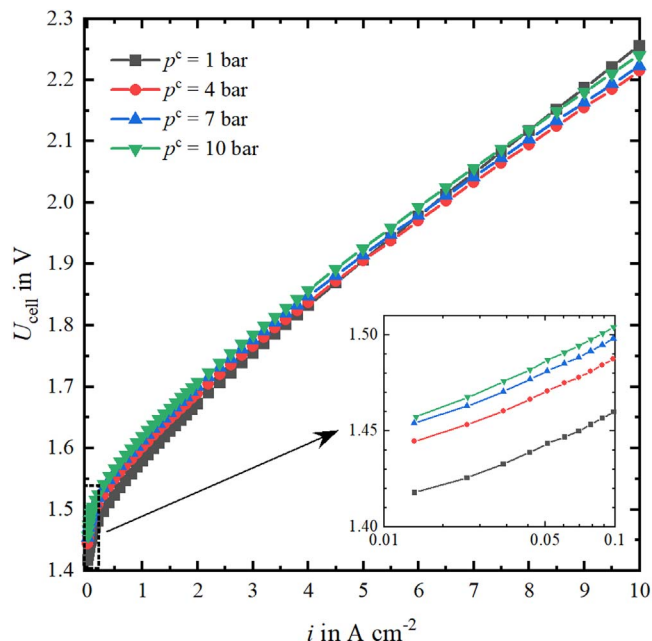

Figure 1. Polarisation behaviour of a 4 cm^2 PEMWE cell, with a Nafion 212 membrane at 80 °C and cathode pressures up to 10 bar. In the zoom of the low current density region (logarithmic), the impact of increasing cathode pressure on the cell voltage becomes clear.

the hydrogen crossover characteristics, which is the focus topic of this contribution.

Polarisation behaviour.—Figure 1 shows the polarisation curves measured with the investigated PEMWE cell at four different cathode pressures. At the maximum current density of 10 A cm^{-2}, the cell voltage remains below 2.25 V. Considering an industrial relevant maximum cell voltage of 2 V, current densities of slightly more than 6 A cm^{-2} can be reached with this setup.

In the low current density region of the polarisation curves (zoom in Fig. 1), the impact of the cathode pressure on the cell voltage according to Nernst's equation is clearly visible. However, the focus of this contribution lays on hydrogen crossover, which is why no further analysis of the cell voltage is given at this point. A more detailed cell voltage breakdown, including the high frequency resistance R_{HF} and iR_{HF}-corrected cell voltage, is given in the Appendix.

Hydrogen crossover at ambient pressure.—The hydrogen crossover measurements at ambient pressure conditions are shown in Fig. 2. The data is divided in three regions, so that the discussion is easier to follow.

Figure 2a) shows the anodic hydrogen in oxygen content ϕ_{H_2}. It is observed that the hydrogen content decreases rapidly at low current densities (region I). This is explained by the linear increase in the amount of evolved oxygen with increasing current density according to Faraday's law, leading to a continuous dilution of the permeated hydrogen (c.f. Eq. 2). At medium current densities (region II), the hydrogen content increases. This trend was already observed in earlier works.[13,17,18,29] Entering region III at high current densities results in a slight decrease of the hydrogen content. To our knowledge, this contribution is a first report on such a course of data.

For the evaluation of the measured data, the hydrogen permeation rate $N_{H_2}^{cross}$ shown in Fig. 2b) (calculated according to Eq. 1), is resolved in the following. Generally, the concentration difference of dissolved hydrogen across the membrane is the driving force for the diffusive hydrogen transport, which is frequently described by Fick's law:[6,7,12,14–16]
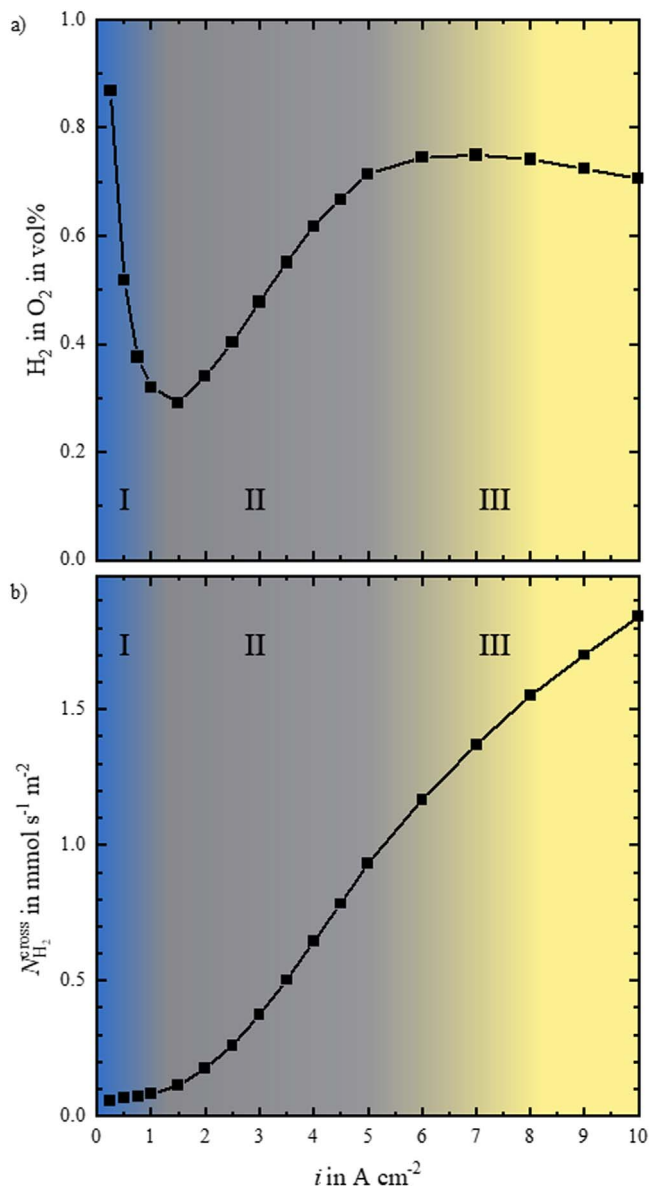
Figure 2. Hydrogen crossover at ambient pressure and 80 °C.

$$N_{H_2}^{diff} = D_{H_2}^{eff} \cdot \frac{c_{H_2}^{*,c} - c_{H_2}^{a}}{\delta_{mem}} \approx D_{H_2}^{eff} \cdot \frac{c_{H_2}^{*,c}(i, k_l, p_{H_2}^{c})}{\delta_{mem}} \qquad [3]$$

Where $D_{H_2}^{eff}$ describes the effective diffusion coefficient of dissolved hydrogen through a wet Nafion membrane and δ_{mem} is the membrane thickness (63 μm for a wet Nafion 212 membrane[12]). Assuming that the hydrogen concentration at the anode $c_{H_2}^{a}$ is negligible, $N_{H_2}^{diff}$ depends mostly on the dissolved, supersaturated hydrogen concentration at the cathode $c_{H_2}^{*,c}$. This supersaturation is a result of mass transport limitations, which depends on the applied current density i and the mass transfer coefficient k_l.[15,16] At zero current, $c_{H_2}^{*,c}$ equals to the hydrogen saturation concentration, which is mainly a function of hydrogen partial pressure $p_{H_2}^{c}$. Consequently, the resulting hydrogen crossover flux at zero current is mainly a function of the hydrogen partial pressure and respectively, of the cathode pressure. This value is the minimum, base amount of permeating hydrogen. In the following, this base diffusion flux will be referred as $N_{H_2}^{diff,0}$.

There are different methods to determine this value (e.g. permeation experiments at zero current,[12,13,30] by electrochemical compensation of permeated hydrogen,[7,8] by linear sweep voltammetry[31] or by extrapolation of the existing data obtained at electrolysis conditions to zero current[13]). Usually, the experimentally obtained values differ slightly from one another.

Trinke et al.[16] investigated the linear relation between $N_{H_2}^{cross}$ and i observed in region I in detail. They concluded that mass transfer resistances in the cathode catalyst layer result in a limited mass transfer of dissolved hydrogen into the gas phase. Since the amount of evolved hydrogen increases linearly with the applied current density (Faraday's law), the dissolved hydrogen concentration increases linearly as well. As a consequence of Fick's law (Eq. 3), the hydrogen crossover flux shows the same linear relationship with current density in this region.

In region II, $N_{H_2}^{cross}$ enters a regime in which a stronger than linear relationship with current density is observed. This effect was already reported in literature[13,18,29] and was recently investigated in a previous work of our group.[17] This functional relationship only agrees with the diffusion approach, if an disproportionate increase of $c_{H_2}^{*,c}$ with i is assumed. This relation can grow stronger than linear, if the reaction front of the hydrogen evolution reaction in the catalyst layer moves towards the membrane[14,32] or other parameters such as the mass transport coefficient k_l or the the diffusion properties in the catalyst layer change. All of these factors result in a continuing growth of $c_{H_2}^{*,c}$ at the interface between the catalyst layer and the membrane, leading to a higher driving force for the cross permeation and eventually to a higher hydrogen crossover flux.

However, the mentioned effects should lead to a further, more than linear growing supersaturation, which would result in a more than linear increase of the hydrogen crossover as well (considering $N_{H_2}^{cross} \approx N_{H_2}^{diff}$). Certainly, this is not observed in region III, but instead a flattening of $N_{H_2}^{cross}$ results in the high current regime. Hence, the earlier introduced, pure diffusive approach with the previous described parameter functionalities, fails to explain the data in at higher current densities.

With such high current densities, increases in temperature and pressure and their impact on hydrogen crossover should be considered. In an earlier study by Trinke et al.,[16] these two and further effects were examined and discussed thoroughly. As the current density increases, more heat is produced, causing the local temperature in the membrane to rise. This causes the diffusion coefficient of hydrogen through Nafion to increase as well and hence, a higher hydrogen crossover flux is expected. However, the current dependence of the crossover flux is found to be stronger than the temperature dependence. The results shown in this work support this finding, since the increase of the hydrogen crossover flux in the high current region III is lower than at medium current densities, as seen in region II. Moreover, Trinke et al.[16] discussed a potential increase of the local hydrogen partial pressure within the cathode with increasing current density. They came to the conclusion that a pressure gradient across the cathode PTL of several 100 bar per cm would be necessary, to explain the observed current dependence of hydrogen crossover. Since such high pressure increases cannot be explained, this approach is insufficient to explain the flattening of the crossover flux observed at high current densities. For this reason, it is assumed that the local increases in temperature and pressure only have a subordinate impact on the current dependence of the hydrogen crossover and therefore do not explain the results either qualitatively or quantitatively.

Another potential explanation for the observed flattening of $N_{H_2}^{cross}$ at high current densities might be another transport mechanism acting in the opposite direction of diffusion. Therefore, the electro-osmotic drag of water comes in mind. During the electrolysis reaction, protons are formed in the anodic half-cell reaction. Due to the electric field between the electrodes, the protons move towards the cathode and drag water molecules with them. Thus, it is obvious that dissolved hydrogen might be carried within the dragged water.[3,15]

This convective hydrogen transport by the electro-osmotic drag of water was already mentioned in literature, but did not receive much attention. Grigoriev et al.[33] were the first to implement this hydrogen transport mechanisms in a mathematical model for PEM water electrolyzers. Schalenbach et al.[3] have simulated hydrogen crossover in PEMWE under various pressure conditions and with different membrane thicknesses and considered the drag of water as well. They came to the conclusion that with the prevailing conditions, diffusion is the dominating transport mechanism and that the impact of the drag on hydrogen crossover is negligible. Trinke et al.[7,15] also emphasized the growing impact of hydrogen and oxygen transport via water drag at increasing current densities. Since diffusion and water drag act in opposite directions in PEMWE, the drag should eventually reduce hydrogen crossover at high current densities.

Generally, the hydrogen transport due to the electro-osmotic drag of water $N_{H_2}^{drag}(x)$ can be described with Eq. 4, where x = 0 marks the interface between membrane and cathode catalyst layer and x reflects the distance to the cathode catalyst layer across the membrane. The net hydrogen crossover flux $N_{H_2}^{cross}$ is then described by Eq. 5.

$$N_{H_2}^{drag}(x) = v_{H_2O}^{drag}(i) \cdot c_{H_2}(x) \qquad [4]$$

$$N_{H_2}^{cross} = N_{H_2}^{diff} - N_{H_2}^{drag} \qquad [5]$$

The velocity of the dragged water is described by $v_{H_2O}^{drag}$ and depends directly on the number of protons transported through the membrane and is therefore a function of the applied current density. Thus, the hydrogen transport via this mechanism is low and slow at small current densities and gains in relevance with increasing current densities. At this point, it is emphasized that the transport via drag does not replace the diffusive transport at high current densities, but that both counteracting mechanisms are coexisting (c.f. Eq. 5).

The dissolved hydrogen concentration at the position x in the membrane is described by $c_{H_2}(x)$. Due to the concentration gradient across the membrane, the hydrogen concentration near the cathode is greater than in the vicinity of the anode. It is therefore expected that the effect of the drag is stronger at the cathode as well. Moreover, the dissolved hydrogen concentration increases with the applied current, which in itself leads to a higher amount of transported hydrogen by the dragged water. A simple calculation in the appendix shows that at higher current densities, hydrogen transport by drag is of the same order of magnitude as the crossover measurement results, which supports this hypothesis.

Following from these assumptions, it is concluded that the amount of dragged hydrogen depends on (i) the amount of dragged water and hence, the current density and (ii) the concentration of dissolved hydrogen within the membrane. According to Eq. 3, the latter can be varied by increasing the hydrogen pressure. For higher cathode pressures it follows that the initial dissolved hydrogen concentration is higher and that the amount of dragged hydrogen already should become noticeable at lower current densities. This hypothesis is evaluated in the next section.

Hydrogen crossover at elevated cathode pressures.—Figure 3a) contains the measured anodic hydrogen content at all investigated cathode pressures. Especially at low current densities, the hydrogen content depends strongly on the cathode pressure, which results in an exceeding of the technical safety criterion of 2 vol% H_2 in O_2 (50% LEL[10]). This is a consequence of the increased base hydrogen permeation flux $N_{H_2}^{diff,0}$ and the low oxygen production rate at the small currents, as described by Eq. 2. In contrast, the increasing oxygen production rate with current density results in a strong dilution of the permeated hydrogen. On account of this, the four curves approach one another at 1 vol%. In the transition area at
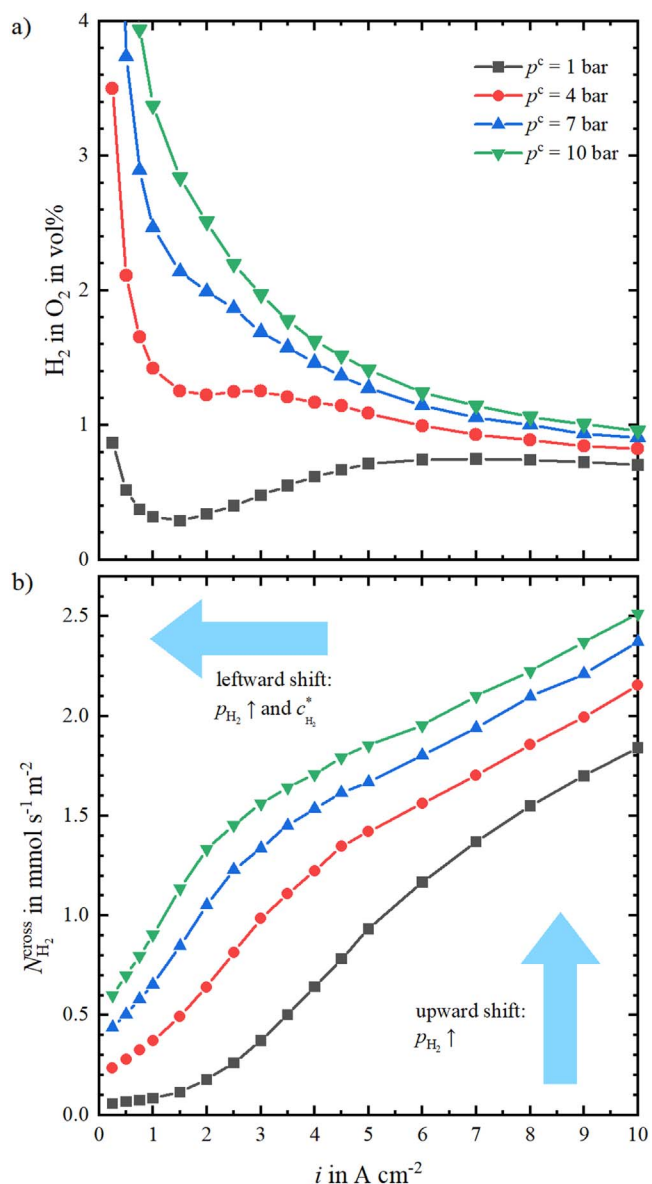

Figure 3. Hydrogen crossover at all cathode pressures and 80 °C. In a) the hydrogen in oxygen content and in b) the hydrogen crossover flux are shown as a function of the current density.

medium current densities, the course of the curve depends on the cathode pressure. At lower pressures, an increase in the hydrogen content is clearly visible and becomes less and less pronounced with increasing pressure. At 15 bar, the hydrogen content has the typical hyperbolic dependence on current density.

A more detailed look into the hydrogen crossover fluxes (Fig. 3b) helps to explain the presented observations. The course of the data at ambient pressure was already discussed in the previous section. This curve is used as a benchmark for comparison in the following discussion.

Generally, the hydrogen crossover fluxes show the same qualitative relation with current density as the benchmark curve. In the beginning, there is a region with a more than linear slope and then the curves flatten at higher current densities. There, the curves seem to be parallel to one another. From a quantitative point of view, the fluxes obtained at higher pressures are shifted (i) upwards to higher permeation fluxes, because of the increasing $N_{H_2}^{diff,0}$ with increasing pressure (c.f. Eq. 3) and (ii) to the left to lower current densities, which results in an earlier flattening of $N_{H_2}^{cross}$.
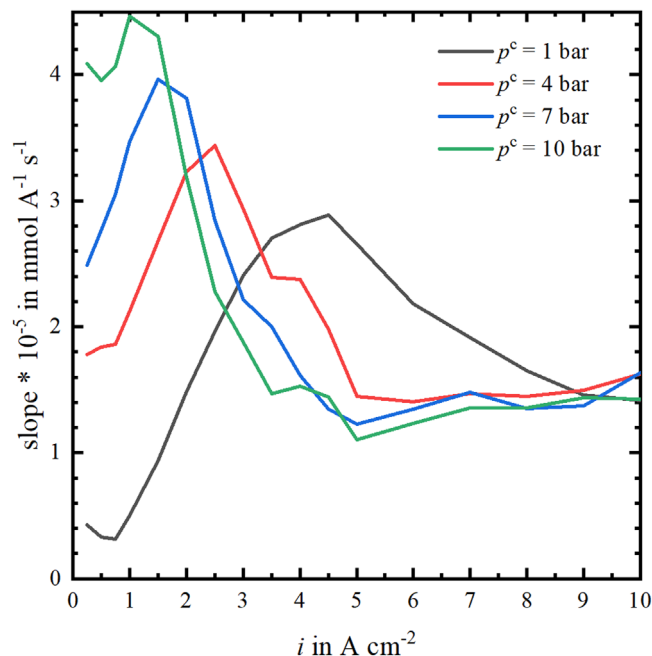
Figure 4. First derivative of the hydrogen crossover fluxes shown in Fig. 3b). With increasing cathode pressure, the maxima shift to lower current densities (1 bar: 4.5 A cm^{-2}, 5 bar: 2.5 A cm^{-2}, 10 bar: 1.5 A cm^{-2}, 15 bar: 1 A cm^{-2}).

For the evaluation of the shift towards lower current densities, the first derivative of $N_{H_2}^{cross}$ is used to assess to slopes (Fig. 4). With respect to the benchmark curve at ambient pressure, the exact same regions as identified in the previous section are visible. The first region up to ~1 A cm^{-2} has a constant slope and corresponds to the linear region I, which was observed previously in Fig. 2b). Then, another region with an increasing slope follows. This region clearly represents the stronger than linear crossover increase (c.f. region II in Fig. 2b). The slope of the ambient pressure curve shows a maximum at ~4.5 A cm^{-2} and decreases afterwards to a value of ~1.2 · 10^{-5} mmol A^{-1} s^{-1}. This reflects the flattening of $N_{H_2}^{cross}$(1 bar) labeled with region III in Fig. 2b).

The other derivatives of $N_{H_2}^{cross}$ at elevated pressures generally show the same trends as the benchmark curve and also pass maxima. From Fig. 4 it becomes clear that the maxima (5 bar: ~2.5 A cm^{-2}, 10 bar: ~1.5 A cm^{-2}, 15 bar: ~1 A cm^{-2}) shift to lower current densities, when the cathode pressure is increased. This mirrors the earlier flattening of the curves (c.f. Fig. 3b). All slopes eventually reach a value of 1.2 · 10^{-5} mmol A^{-1} s^{-1}, which matches to the parallel course of all $N_{H_2}^{cross}$ at high current densities, as seen in Fig. 3b).

These findings fit well to the previous hypothesis, in which it was assumed that the flattening of $N_{H_2}^{cross}$ at high current densities is a result of the electro-osmotic drag of water. This convectively transported water carries an increasing amount of dissolved hydrogen back to the cathode. If this hypothesis is expanded to elevated cathode pressures, it is assumed that the impact of the drag must begin at lower current densities, because the overall amount of dissolved hydrogen is higher and leads to a higher back transport (c.f. Eq. 4). Therefore, $N_{H_2}^{drag}$ should also increase with pressure in exactly this point. In relation to the presented data, it is assumed that the earlier flattening of $N_{H_2}^{cross}$ and the resulting shift of the inflection point to lower current densities (c.f. Fig. 4) supports this hypothesis.

Besides the curve flattening, the parallel course of $N_{H_2}^{cross}$ in the high current density region is another remarkable characteristic. Apparently, the drag counteracts the disproportionate increase of the

hydrogen crossover flux at higher current densities, so that the fluxes eventually increase linearly again. Moreover, it is questionable how long the increase in $N_{H_2}^{cross}$ will proceed. Since the infinite growth of $c_{H_2}^{*,c}$ in the cathode catalyst layer is questionable, there might be a kind of natural limit at some point, which perhaps leads to a saturation of $N_{H_2}^{cross}$. Further, it might be possible that the drag increases so much at even higher cathode pressures, that the hydrogen crossover flux starts to decrease at high current densities.

Summary & Conclusion

In this study, the polarisation behaviours and the hydrogen crossover in PEMWE cells with a thin Nafion 212 membrane at current densities up to 10 A cm^{-2} and cathode pressures up to 10 bar were investigated. At the maximum current density, the resulting cell voltage was only ~2.25 V. Further, no hints for significant mass transport limitations were observed.

The analysis of the hydrogen crossover characteristics was divided in two section (ambient pressure and elevated pressures). The evaluation at ambient pressure revealed that the hydrogen crossover flux generally increases with current density. Further, it was observed that the hydrogen crossover flux passes through a linear and a more than linear region, before flattening out at high current densities. It is assumed that the transition of the slopes at high currents is a first experimental indicator that the hydrogen transport due to the electro-osmotic drag of water competes with the diffusive hydrogen transport. Eventually, these two competing transport modes lead to a lower total increase in the hydrogen crossover flux over the investigated current density range, than expected from a pure diffusive approach.

The crossover analysis at increased cathode pressures revealed that the hydrogen crossover flux not only increases with cathode pressure, but also that the curve flattening begins at lower current densities. It was assumed that this is as well a result of the hydrogen transport via dragged water, because the hydrogen concentration within the membrane increases with pressure.

The presented results indicate that a pure diffusive approach is insufficient to explain experimentally determined hydrogen crossover data, especially at high current densities, and that presumably negligible effects, such as the effect of the electro-osmotic drag on hydrogen crossover, should be considered in future. Further, the results emphasize that the consideration of this transport mode becomes essential, when diffusion is not the dominating gas transport mechanism anymore. This occurs especially when thick membranes are used or as in this study, when high current densities are applied and the hydrogen concentrations are high.

Another aspect to be considered is the impact of the electro-osmotic drag on oxygen crossover. In this study, it was assumed that the drag attenuates the net hydrogen crossover, since it opposes to the hydrogen diffusion direction. Consequently, the drag should enhance oxygen crossover, because it acts in the same direction as the oxygen diffusion. In order to investigate this in more detail, methods for the precise measurement of oxygen crossover during electrolysis have to be established. Further, a model description of the dissolved gas concentration profiles across the catalyst layers and the membrane could help to elucidate the impact of the electro-osmotic drag on both gas crossovers.

Estimation of Electro-osmotically Dragged Hydrogen

As the hydrogen concentration depends on the position in the membrane, a one dimensional model is necessary for a more precise calculation of the diffusive and convective hydrogen fluxes through

the membrane. The formulation of such a model is quite extensive, which is why only a very simple estimation (neglecting the dependence on the position) of the dragged hydrogen flux is given here to support our hypothesis, that that the electro-osmotic drag of water at elevated current densities carries a significant amount of hydrogen back to the cathode.

As shown previously, the convective hydrogen transport is calculated as follows (c.f. Eq. 4):

$$N_{H_2}^{drag} = \underbrace{\frac{n_{drag} \cdot i}{F \cdot c_{H_2O}}}_{v_{H_2O}} \cdot c_{H_2}^* \qquad [\text{A}\cdot1]$$

First, the dissolved hydrogen concentration $c_{H_2}^*$ at an average hydrogen crossover flux of $N_{H_2}^{cross} = 0.5$ mmol s^{-1} m^{-2} is calculated from Fick's first law of diffusion (c.f. Eq. 3). With a wet membrane thickness $\delta_{mem} = 63$ μm[12] and an effective diffusion coefficient $D_{H_2}^{eff} = 2.9 \cdot 10^{-9}$ m^2 s^{-1},[14] it follows:

$$c_{H_2}^* = N_{H_2}^{cross} \cdot \frac{\delta_{mem}}{D_{H_2}^{eff}} = 10862 \frac{\text{mmol}}{\text{m}^3} \qquad [\text{A}\cdot2]$$

In the next step, the concentration of water $c_{H_2O} = 0.054$ mol cm^{-3} is calculated from the ratio of the density at 80 °C $\rho = 0.972$ g cm^{-3} and the molar mass $M_{H_2O} = 18$ g mol^{-1}.

Lastly, at a current density of 5 A cm^{-2} and a mean drag coefficient[40,41] $n_{drag} = 2.5$, a dragged hydrogen flux of $N_{H_2}^{drag} \approx 0.26$ mmol s^{-1} m^{-2} is calculated according to Eq. A·1.

As this value has the same order of magnitude as the crossover measurement results shown in Fig. 2b), it supports the hypothesis, that the convective hydrogen transport via drag can counteract the diffusive transport.

Appendix

Cell voltage analysis.—A detailed cell voltage analysis was omitted in the main part of this contribution, because the focus lays on hydrogen crossover at high current densities in PEMWE. However, the polarisation behaviour and major voltage loss sources at such high current densities should be considered for a complete evaluation of a PEMWE cell. Therefore, the analysis is made up for at this point.

Figure A·1a) shows the measured cell voltage as a function of the applied current density. The dependence on the pressure is clearly visible at low current densities. There, the voltage increases with increasing cathode pressure. Above 6 A cm^{-2}, no clear relation between the cell voltage and the pressure is visible anymore. At the maximum current density of 10 A cm^{-2}, the cell voltage is around 2.25 V.

Möckl et al.[34] investigated the thermal limitations of PEMWE cells operated at high current densities as well. In the study, Nafion membranes of different thicknesses (117, 212 and XL) were compared. The cell with Nafion 212 achieved an almost identical cell voltage (~2.25 V) at 10 A cm^{-2} compared to the present work. It is also striking that the current-voltage relation appears to remain linear at such high currents. This indicates that PEMWE cells are not limited by water transport to the reaction zone or a product accumulation at either electrode. In Möckl's work,[34] significant mass transport limitations start at around 12 A cm^{-2}. The excellent cell performance reported in this work is mainly a result of the low protonic resistance of the thin membrane. For a thicker Nafion 117 membrane at 80 °C, cell voltages of 2.2 V are already reached below 5 A cm^{-2}.[13,34,35]

In this work, the ohmic cell resistance was measured with electrochemical impedance spectroscopy, by determining the high frequency resistance R_{HF}. The respective results are shown in Fig. A·1b). The values reported here (61 … 68 mΩ cm^2) are slightly higher than those reported in a previous study,[17] although the measurement and the setup are almost identical. One potential explanation may be

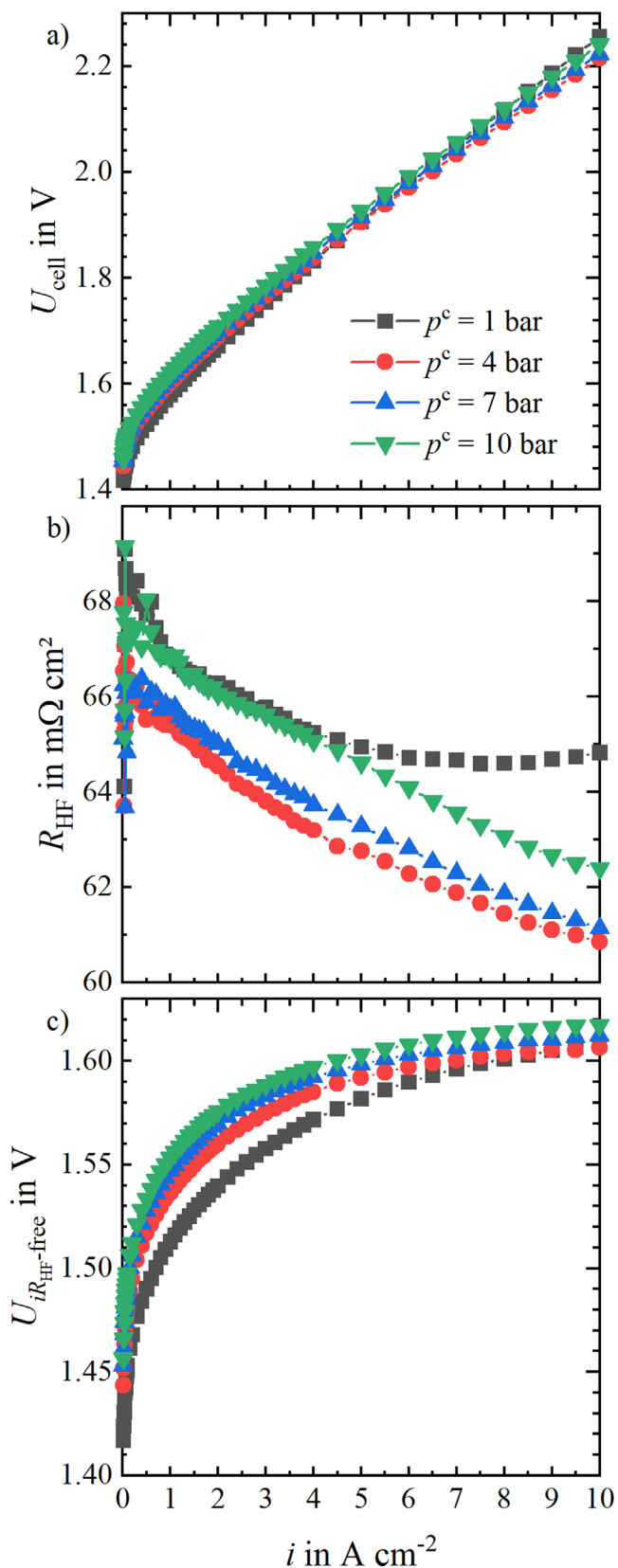**Figure A·1.** Cell voltage analysis of a PEM water electrolysis cell with Nafion 212 at 80 °C. The measured cell voltage is shown in a), b) shows the high frequency resistance R_{HF} and c) presents the iR_{HF}-free cell voltage.

found in differences of the setup. The main setup difference to the previous work is the used anode PTL (1 mm Ti-fiber vs. 350 μm Ir-coated Ti-fibers). In accordance to the works of Liu et al.,[36,37] the

electrochemical performance of cells with an iridium coated PTL is better than with an uncoated one. Iridium prevents the corrosion titanium, leading to a lower PTL resistance and thus, a lower contribution of the PTL to R_{HF}.

Further, it is assumed that the main part of the ohmic cell resistance can be attributed to the ohmic losses due to proton transport through the membrane. Generally, R_{HF} is decreasing with increasing current density. This trend was observed previously and was explained with the reduction of ohmic resistances due to temperature increases at increasing current densities.[17,38,39] This was evidenced with the test station. Temperature probes were placed at the electrode endplates directly below the flow field. Compared to low current densities, a temperature increase of 2 K to 3 K was measured at 10 A cm^{-2} at the anode endplate.

Although the differences between the curves are small ($\leqslant$4 mΩ cm^2), a dependence on pressure is observed. R_{HF} is the lowest at 4 bar. This trend was already observed and discussed previously.[17] In the referred study, the minimum of R_{HF} was measured at a similar cathode pressure level (5 bar).

As a next step of the voltage loss analysis, the ohmic voltage losses are subtracted from the measured cell voltage. The resulting iR_{HF}-corrected cell voltage is shown in Fig. A·1c). Here, it is observed that the iR_{HF}-corrected voltages increase and the distances between the curves decrease with cathode pressure. Both trends can be explained with the logarithmic dependence of the voltage on the hydrogen pressure according to Nernst's equation.

In principle, further voltage losses, such as mass transport losses, are expected at high current densities. In order to calculate these, a Tafel analysis, in which the iR-corrected data is linearly fitted with a logarithmic current axis, has to be performed. For this purpose, the measured data must be reliable, especially at low current densities (between 10 … 100 mA cm^{-2}). Hence, high accuracies are needed. Since a very powerful current booster (designed for 100 A) was used for this study, the required accuracy cannot be achieved at the low current densities. For this reason, the Tafel analysis is not performed and the voltage loss break down ends here. At this point, we would like to appeal to our readers, who carry out similar measurements and analyses, to always pay attention to the measuring accuracy of their used devices. This is the only way to check whether the measured data is reliable, suitable for a detailed analysis and worth for sharing with the scientific community.

ORCID

Agate Martin https://orcid.org/0000-0003-4673-1135
Patrick Trinke https://orcid.org/null
Boris Bensmann https://orcid.org/0000-0001-8685-7192
Richard Hanke-Rauschenbach https://orcid.org/0000-0002-1958-307X

References

1. K. Ayers, N. Danilovic, K. Harrison, and H. Xu, *Electrochem. Soc. Interface*, **30**, 67 (2021).
2. K. Ayers, *Curr. Opin. Elechtrochem.*, **18**, 9 (2019).
3. M. Schalenbach, M. Carmo, D. L. Fritz, J. Mergel, and D. Stolten, *Int. J. Hydrogen Energ.*, **38**, 14921 (2013).
4. M. Schalenbach, *Int. J. Hydrogen Energ.*, **41**, 729 (2016).
5. M. Schalenbach and D. Stolten, *Electrochim. Acta*, **156**, 321 (2015).
6. H. Ito, N. Miyazaki, M. Ishida, and A. Nakano, *Int. J. Hydrogen Energ.*, **41**, 20439 (2016).
7. P. Trinke, B. Bensmann, S. Reichstein, R. Hanke-Rauschenbach, and K. Sundmacher, *J. Electrochem. Soc.*, **163**, F3164 (2016).
8. B. Bensmann, R. Hanke-Rauschenbach, and K. Sundmacher, *Int. J. Hydrogen Energ.*, **39**, 49 (2014).
9. F. Scheepers, M. Stähler, A. Stähler, E. Rauls, M. Müller, M. Carmo, and W. Lehnert, *Energies*, **13**, 612 (2020).
10. H. Janssen, J. C. Bringmann, B. Emonts, and V. Schroeder, *Int. J. Hydrogen Energ.*, **29**, 759 (2004).
11. S. A. Grigoriev, P. Millet, S. V. Korobtsev, V. I. Porembskiy, M. Pepic, C. Etievant, C. Puyenchet, and V. N. Fateev, *Int. J. Hydrogen Energ.*, **34**, 5986 (2009).
12. M. Schalenbach, T. Hoefner, P. Paciok, M. Carmo, W. Lueke, and D. Stolten, *J. Phys. Chem. C*, **119**, 25145 (2015).
13. M. Bernt, J. Schröter, M. Möckl, and H. A. Gasteiger, *J. Electrochem. Soc.*, **167**, 124502 (2020).
14. P. Trinke, G. P. Keeley, M. Carmo, B. Bensmann, and R. Hanke-Rauschenbach, *J. Electrochem. Soc.*, **166**, F465 (2019).
15. P. Trinke, P. Haug, J. Brauns, B. Bensmann, R. Hanke-Rauschenbach, and T. Turek, *J. Electrochem. Soc.*, **165**, F502 (2018).
16. P. Trinke, B. Bensmann, and R. Hanke-Rauschenbach, *Int. J. Hydrogen Energ.*, **42**, 14355 (2017).
17. A. Martin, P. Trinke, M. Stähler, A. Stähler, F. Scheepers, B. Bensmann, M. Carmo, W. Lehnert, and R. Hanke-Rauschenbach, *J. Electrochem. Soc.*, **169**, 14502 (2022).
18. M. Stähler, A. Stähler, F. Scheepers, M. Carmo, W. Lehnert, and D. Stolten, *Int. J. Hydrogen Energ.*, **45**, 4008 (2020).
19. S. Garbe, E. Samuelsson, T. J. Schmidt, and L. Gubler, *J. Electrochem. Soc.*, **168**, 104502 (2021).
20. B. Bensmann, A. Rex, and R. Hanke-Rauschenbach, *Curr. Opin. Chem. Eng.*, **36**, 100829 (2022).
21. Fraunhofer Institute for Solar Energy Systems ISE, *Fraunhofer ISE—Annual Report 2020/2021* (Freiburg, Germany) (2021).
22. N. Li, S. S. Araya, X. Cui, and S. K. Kær, *J. Power Sources*, **473**, 228617 (2020).
23. N. Li, S. S. Araya, and S. K. Kær, *J. Power Sources*, **434**, 226755 (2019).
24. S. A. Grigoriev, K. A. Dzhus, D. G. Bessarabov, and P. Millet, *Int. J. Hydrogen Energ.*, **39**(35), 20440 (2014).
25. ProtonOnSite, Technical Specifications H Series Hydrogen Generation System: PD-0600-0062 Rev F https://www.protononsite.com/sites/default/files/2017-04/PD-0600-0062%20Rev%20F.pdf.
26. ProtonOnSite, Technical Specifications M400 Hydrogen Generation System: PD-0600-0122 REV A https://protonenergy.com/sites/default/files/2017-06/PD-0600-0122%20REV%20A.pdf.
27. Proton Energy Systems, Technical Specifications Hogen Hydrogen Generation Systems: S Series Hydrogen Generators http://hmagrp.com/wp-content/uploads/2016/09/HOGEN-S-Series.pdf.
28. A. Martin, D. Abbas, P. Trinke, T. Böhm, M. Bierling, B. Bensmann, S. Thiele, and R. Hanke-Rauschenbach, *J. Electrochem. Soc.*, **168**, 94509 (2021).
29. C. Klose, P. Trinke, T. Böhm, B. Bensmann, S. Vierrath, R. Hanke-Rauschenbach, and S. Thiele, *J. Electrochem. Soc.*, **165**, F1271 (2018).
30. F. Barbir, *Sol. Energy*, **78**, 661 (2005).
31. P. Pei, Z. Wu, Y. Li, X. Jia, D. Chen, and S. Huang, *Appl. Energy*, **215**, 338 (2018).
32. P. Trinke, *Experimental and Model-based Investigations on Gas Crossover in Polymer Electrolyte Membrane Water Electrolyzers* (Hannover, Germany) (2021).
33. S. A. Grigoriev, A. A. Kalinnikov, P. Millet, V. I. Porembsky, and V. N. Fateev, *J. Appl. Electrochem.*, **40**, 921 (2010).
34. M. Möckl, M. Bernt, J. Schröter, and A. Jossen, *Int. J. Hydrogen Energ.*, **45**, 1417 (2020).
35. A. Villagra and P. Millet, *Int. J. Hydrogen Energ.*, **44**, 9708 (2019).
36. C. Liu, M. Carmo, G. Bender, A. Everwand, T. Lickert, J. L. Young, T. Smolinka, D. Stolten, and W. Lehnert, *Electrochem. Commun.*, **97**, 96 (2018).
37. C. Liu et al., *Adv. Energy Mater.*, **11**, 2002926 (2021).
38. T. Schuler, T. J. Schmidt, and F. N. Büchi, *J. Electrochem. Soc.*, **166**, F555 (2019).
39. M. Suermann, T. J. Schmidt, and F. N. Büchi, *Electrochim. Acta*, **211**, 989 (2016).
40. T. A. Zawodzinski, J. Davey, J. Valerio, and S. Gottesfeld, *Electrochim. Acta*, **40**, 297 (1995).
41. Z. Luo, Z. Chang, Y. Zhang, Z. Liu, and J. Li, *Int. J. Hydrogen Energ.*, **35**, 3120 (2010).